Journal of ELECTRONIC MATERIALS, Vol. 46, No. 10, 2017
DOI: 10.1007/s11664-017-5641-3

Composites Based on Core–Shell Structured HBCuPc@CNTs-Fe_3O_4 and Polyarylene Ether Nitriles with Excellent Dielectric and Mechanical Properties

ZEJUN PU,[1,3] JIACHUN ZHONG,[1] and XIAOBO LIU[2]

1.—College of Materials Science and Engineering, Sichuan University of Science and Engineering, Zigong 643000, China. 2.—High Temperature Resistant Polymer and Composites Key Laboratory of Sichuan Province, University of Electronic Science and Technology of China, Chengdu 610054, China. 3.—e-mail: puzejunuestc@163.com

Core–shell structured magnetic carbon nanotubes (CNTs-Fe_3O_4) coated with hyperbranched copper phthalocyanine (HBCuPc) (HBCuPc@CNTs-Fe_3O_4) hybrids were prepared by the solvent-thermal method. The results indicated that the HBCuPc molecules were decorated on the surface of CNTs-Fe_3O_4 through coordination behavior of phthalocyanines, and the CNTs-Fe_3O_4 core was completely coaxial wrapped by a functional intermediate HBCuPc shell. Then, polymer-based composites with a relatively high dielectric constant and low dielectric loss were fabricated by using core–shell structured HBCuPc@CNTs-Fe_3O_4 hybrids as fillers and polyarylene ether nitriles (PEN) as the polymer matrix. The cross-sectional scanning electron microscopy (SEM) images of composites showed that there is almost no agglomeration and internal delamination. In addition, the rheological analysis reveals that the core–shell structured HBCuPc@CNTs-Fe_3O_4 hybrids present better dispersion and stronger interface adhesion with the PEN matrix than CNTs-Fe_3O_4, thus resulting in significant improvement of the mechanical, thermal and dielectric properties of polymer-based composites.

Key words: Polymer-based composites, core–shell structure, rheology, mechanical properties, dielectric properties

INTRODUCTION

High-technology electrical/electronic devices require high permittivity materials (known as high-k materials) with excellent comprehensive performance.[1–4] It is well known that a high-k material can store more electric energy than a lower one. As a result, the efficiency of electronic devices can be obviously improved. High-k inorganic ceramics materials have been widely used in many civilian and military applications for their unique properties.[5,6] However, the light weight and miniaturization trend of electric devices calls for replacing the traditional discrete passive components (such as capacitors (C), resistors (R) and inductors (L)) with embedded passives, namely, the passive components are integrated into a substrate as a thin film layer.[7] In recent years, many works have been reported on fabricating composites with high-k by the combination of dissimilar materials, especially for high-k polymer-based composites.[8,9] The use of different dissimilar materials in the polymer-based composites often creates poor dispersion and interfaces, which have a crucial influence on final dielectric properties and other performances of the composites. Therefore, it is very important to improve the efficient dispersion of individual fillers and their chemical affinity with the surrounding polymer matrix. Up to now, many ceramic/polymer-based composites have been used in electronic fields.[10–13] However, to achieve a higher dielectric

(Received February 11, 2017; accepted June 2, 2017; published online June 16, 2017)
Zejun Pu and Jiachun Zhong contributed equally to this work.

constant, a large amount of ceramic fillers (the concentration of the ceramic fillers is often over 50 vol.%) needs to be filled into the polymer matrix, which will dramatically increase the dielectric losses and brittleness of the composites. Therefore, polymer/modified conductive fillers (such as carbon black,[14] carbon nanotubes,[15,16] graphene,[17,18,] etc.) composites have been identified as a promising approach to achieve the combination of the two outstanding dielectric and mechanical properties. In addition, the dielectric properties of the polymer-based composites can be magically improved by adding a small amount of conductive fillers.

Conductive fillers, especially the carbon nanotubes (CNTs), have attracted considerable attention for their superior electric conductivity.[19–21] Very recently, many works have been reported on improving the dielectric properties of the polymer-based composites by adding CNTs into the polymer matrix. However, the CNTs have a poor compatibility with the polymer matrix, and the CNTs are very prone to agglomerate in the matrix due to their strong intertube van der Waals' forces. Even though the permittivity of the polymer-based composites did dramatically increase with the increasing CNTs loading, their dielectric losses also rise for the high leakage current caused by the direct connection among CNTs. To address this issue, Yang et al.[22] grafted 4-aminophenoxyphthalonitrile (4-APN) layers on the surface of CNTs, and then prepared nitrile functionalized CNTs/polyarylene ether nitriles (CNTs-CN/PEN) composites to investigate the influence of 4-APN grafting layers on their rheological and thermal behaviors. Chen et al.[23] fabricated amino-modified-CNT (NH_2-MWNT)/polyimide (NH_2-MWNT/PI) flexile composite films with a sandwich structure, and the obtained polymer-based composites containing 10 wt.% NH_2-MWNT possessed a permittivity of 31 and dielectric loss of 0.022 at 1 kHz. The surface modification helps the homogeneous dispersion of CNTs in the polymer matrix, and the dependency of permittivity on frequency attenuated and dielectric loss was lowered to below 0.05 (at 1 kHz).

As a versatile high-performance engineering thermoplastic, polyarylene ether nitriles (PEN) have wide applications owning to their high thermal stability and mechanical strength, excellent radiation and chemical stability, good dielectric properties and high electrical breakdown strength, etc.[24,25] In addition, the permittivity of pure PEN film is about 4, while the dielectric loss is less than 0.02 (1 kHz). Such a low dielectric loss of the PEN film is too large for practical application. To achieve better dispersion and an inorganic–organic interface, we report a strategy to fabricate core–shell structured magnetic carbon nanotubes (CNTs-Fe_3O_4) coated with hyperbranched copper phthalocyanine (HBCuPc) (HBCuPc@CNTs-Fe_3O_4) *via* a simple solvent-thermal method. Especially, the introduction of organic semiconductor layers on the surface of CNTs is also an effective way to avoid the formation of the conductive network in the polymer-based composites. Thus, PEN composites containing different contents of functionalized magnetic CNT were prepared by solution-casting method and systematically investigated for their rheological and dielectric properties. The different functionalized magnetic CNTs (CNTs-Fe_3O_4 and HBCuPc@CNTs-Fe_3O_4) can result in thermal and rheological differences that can in turn reveal the relationship between structures and properties of PEN-based composites.

EXPERIMENTAL

Materials

CNTs (purity: >95%) were supplied by Chengdu Organic Chemicals Co., Ltd. CNTs-Fe_3O_4 was prepared according to our previous report.[26] $CuAc_2{\cdot}H_2O$ and ammonium molybdate were purchased from Kelong reagent Co. Ltd., Chengdu, China. 1,3,5-Tri-(3,4-dicyanophenoxy) benzene (TPH) and hyperbranched copper phthalocyanines (HBCuPc) were synthesized in our lab.

Preparation of HBCuPc@CNTs-Fe_3O_4 Hybrids

The core–shell structured HBCuPc@CNTs-Fe_3O_4 hybrids were fabricated by the solvent-thermal method. In the first step, 0.2 g CNTs-Fe_3O_4 particles and 0.2 g HBCuPc were dispersed in DMAc (30 mL) with the help of violent ultrasonics at 80°C for 30 min, followed by the addition of $CuAc_2{\cdot}H_2O$ (0.8 mmol) and ammonium molybdate (40 mg) to form a dark solution in an ultrasonic bath. Then, the mixture suspension was transferred into a teflon-lined stainless-steel autoclave and maintained at 200°C for 15 h. The obtained products were washed with distilled water and ethanol for several times, and then dried under vacuum at 80°C for 6 h.

Fabrication of PEN/HBCuPc@CNTs-Fe_3O_4 Composite Films

PEN/HBCuPc@CNTs-Fe_3O_4 and PEN/CNTs-Fe_3O_4 composites were fabricated according to the method described in our paper.[27] The mass fraction of HBCuPc@CNTs-Fe_3O_4 was fixed at 0 wt.%; 2 wt.%; 4 wt.%; 6 wt.%; 8 wt.%; and 10 wt.%. For a parallel comparison of CNTs-Fe_3O_4 and HBCuPc@CNTs-Fe_3O_4 in PEN matrix, in this paper, the content of CNTs-Fe_3O_4 in the PEN/HBCuPc@CNTs-Fe_3O_4 composites was calculated by TGA analysis results according to the Eq. 1:

$$wt_{\mathrm{CNTs-Fe_3O_4}}\% = m_{\mathrm{HBCuPc@CNTs-Fe_3O_4}} \times (1 - \mathrm{grafting}\%) \Big/ \left(m_{\mathrm{HBCuPc@CNTs-Fe_3O_4}} + m_{\mathrm{PEN}}\right). \quad (1)$$

Thus, the corresponding mass fraction of CNTs-Fe_3O_4 in PEN/CNTs-Fe_3O_4 composites can be

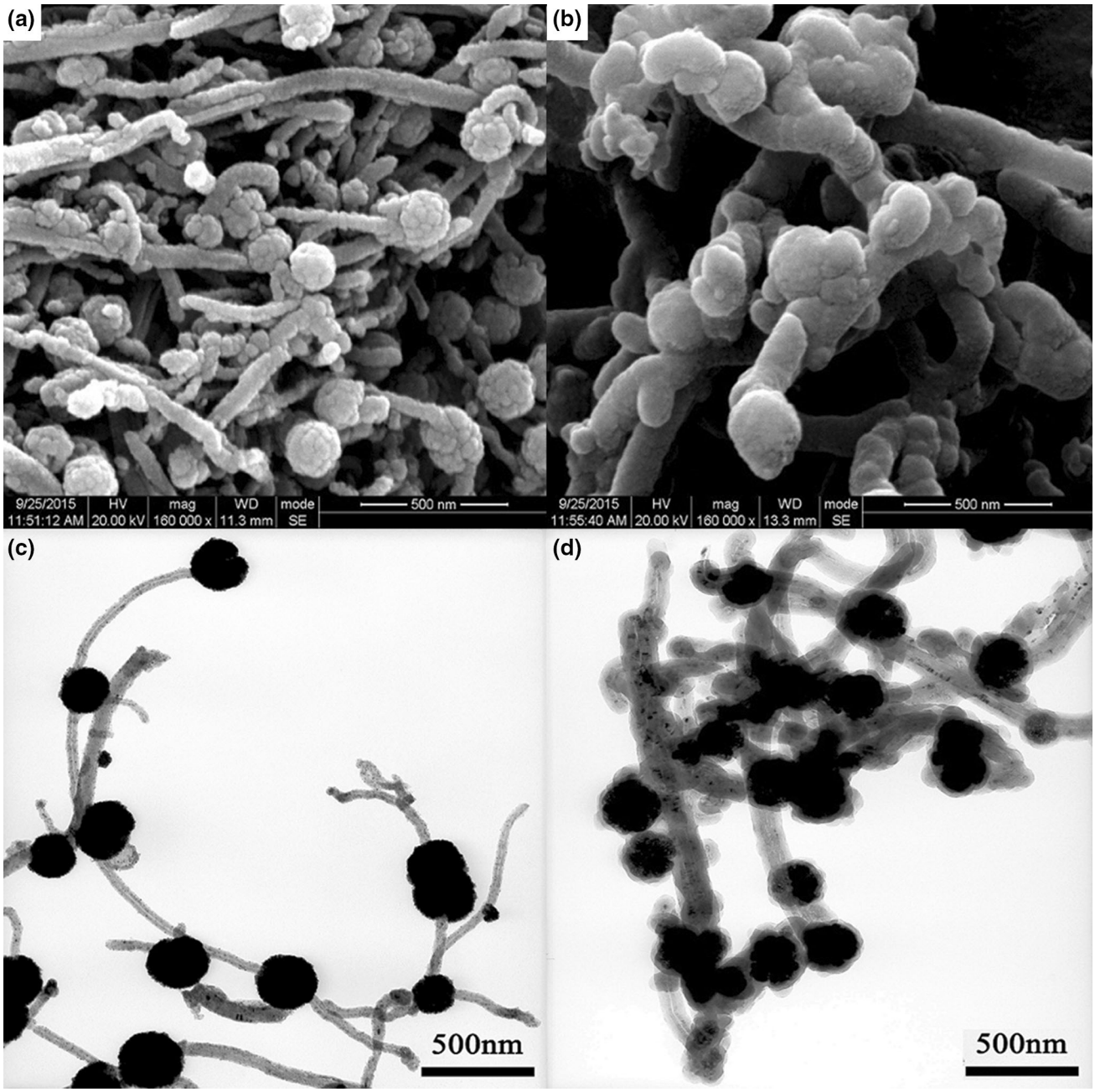

Fig. 1. SEM images of (a) CNTs-Fe_3O_4 and (b) HBCuPc@CNTs-Fe_3O_4; TEM images of (c) CNTs-Fe_3O_4 and (d) HBCuPc@CNTs-Fe_3O_4.

assured identically as 0 wt.%; 1.1 wt.%; 2.2 wt.%; 3.3 wt.%; 4.4 wt.%; and 5.5wt.%.

Characterization

Scanning electron microscopy (SEM) was performed on a JEOL JSM-6490LV at 20 kV. Transmission electron microscopy (TEM) was acquired using a FEI Tecnai G2 F20 electron microscope at 100 kV. Fourier transform infrared (FTIR) spectra were recorded on a Shimadzu 8000S spectrophotometer. X-ray photoelectron spectroscopy (XPS) was carried out with an ESCA-LAB 250 electron spectrometer from Thermo Fisher Scientific, USA. Dynamical rheological measurements of composite films were carried out using a rheometer (Rheometer AR-G2) equipped with parallel-plate geometry (25 mm diameter). Differential scanning calorimetry (DSC) analysis was carried out on a TA Instruments DSC Q100 modulated thermal analyzer under nitrogen atmosphere. Thermogravimetric analysis (TGA) was performed on a TA instrument TGA Q50 series analyzer system under a nitrogen atmosphere. Mechanical properties of PEN composites films were performed by a SANS CMT6104 Series Desktop Electromechanical Universal

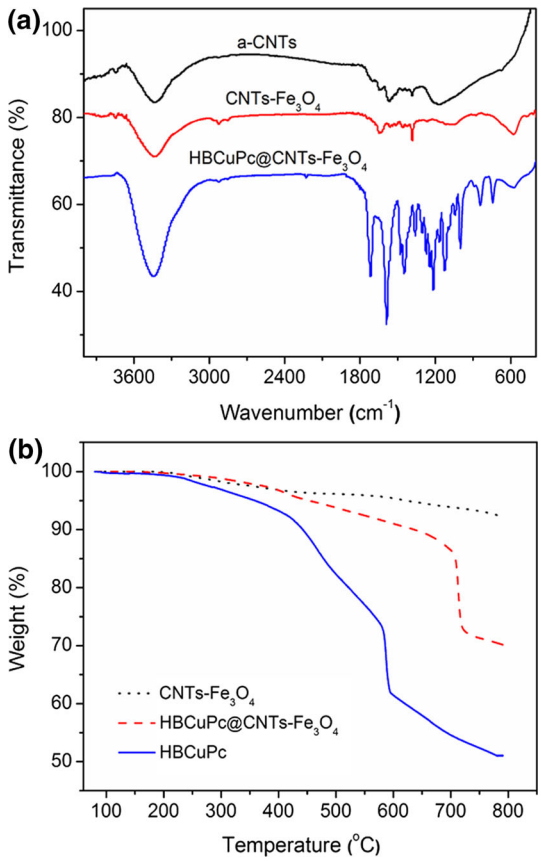

Fig. 2. (a) FT-IR spectra of a-CNTs, CNTs-Fe_3O_4 and HBCuPc@CNTs-Fe_3O_4; (b) TGA curves of CNTs-Fe_3O_4, HBCuPc@CNTs-Fe_3O_4 and HBCuPc.

Testing Machine at room temperature. Dielectric properties of PEN composite films were monitored according to the ASTM D150 on a TH 2819A precision LCR meter.

RESULTS AND DISCUSSION

Characterization of HBCuPc@CNTs-Fe_3O_4 Hybrids

Figure 1a and b show the morphologies of CNTs-Fe_3O_4 and HBCuPc@CNTs-Fe_3O_4, where the HBCuPc@CNTs-Fe_3O_4 presents obvious differences in the morphology and structure in comparison to the CNTs/Fe_3O_4. The different morphologies and structures of the various functionalized CNTs would affect the reinforcement efficiency, processing procedure and properties of the composites. It can be seen from Fig. 1a that most of the CNTs have been coated with magnetic Fe_3O_4 microspheres, and the distribution of magnetic Fe_3O_4 microspheres on the CNTs surface is relatively uniform; while the surface of the HBCuPc@CNTs-Fe_3O_4 is obviously coated with a layer of organic compounds, and the average diameter is also bigger than that of CNTs-Fe_3O_4. The results demonstrated that the HBCuPc molecules were successfully attached to the surface of CNTs-Fe_3O_4, which well matches the TEM images of the functional CNTs. In Fig. 1c, the TEM image shows that the CNTs-Fe_3O_4 has a smooth and clean surface. In contrast, the TEM image of HBCuPc@CNTs-Fe_3O_4 presents that the compact organic layer was completely coated on the surface of CNTs-Fe_3O_4, and the observed organic layer has an thickness of approximately 20–30 nm, which is more beneficial for the physical entanglement of HBCuPc shell with the PEN matrix and enhancement of the interfacial compatibility between CNTs-Fe_3O_4 and the PEN matrix. In short, the organic HBCuPc shell acts as a "bridge" and improves the interfacial adhesion of the inorganic-organic phase, thereby enhancing the compatibility between CNTs-Fe_3O_4 and the PEN matrix.

The surface modification of CNTs-Fe_3O_4 was firstly investigated by FTIR. As shown in Fig. 2a, the strong band at 580 cm^{-1} corresponds to the Fe–O vibration absorption peak.[28] The absorption bands at 1605 cm^{-1}, 1123 cm^{-1}, 1089 cm^{-1}, 905 cm^{-1}, and 832 cm^{-1} correspond to phthalocyanine skeletal and metal–ligand vibrations, respectively.[29–31] In addition, a characteristic absorption band at 2230 cm^{-1} belonging to the symmetric stretching vibration of nitrile groups (-CN) was clearly observed in HBCuPc@CNTs-Fe_3O_4 particles, which demonstrated that the HBCuPc has been coated onto the CNTs-Fe_3O_4 surface. The results were in accordance with the previous work.[32]

TGA analysis was used to estimate the content of organic phase in HBCuPc@CNTs-Fe_3O_4 particles. As shown in Fig. 2b, the TGA curves of CNTs-Fe_3O_4 particles showed a weight loss of 7.9 wt.%, when the temperature reached 800°C. However, the HBCuPc and HBCuPc@CNTs-Fe_3O_4 particles showed a noticeable weight loss in the temperature range of 400–750°C, which is attributed to the loss of surface-coated HBCuPc, so the content of the phthalocyanine decorated on the surface of CNTs-Fe_3O_4 is estimated as 45 wt.%.

The chemical composition of the HBCuPc@CNTs-Fe_3O_4 particles was further verified by XPS. As can be seen in Fig. 3a, the fully scanned spectra not only presented the elements C, O and Fe in the sample, but also revealed the elements Cu and N present on the hybrids. In Fig. 3b, there are two slight symmetric peaks in the Cu 2p region. The peak at 933.3 eV corresponded to the Cu $2p_{3/2}$, and the other at 953 eV was assigned to Cu $2p_{1/2}$, indicating a normal state of Cu^{2+} in the hybrid particles. In Fig. 3c, two intense peaks for the Fe $2p_{3/2}$ and Fe $2p_{1/2}$ signals at 711.2 eV and 724.5 eV can be seen, indicating the presence of Fe_3O_4. Besides, a lower peak at 711.4 eV was observed, which corresponded to the Fe–N, and confirmed the formation of iron phthalocyanine (FePc).[33] All the above results demonstrated that the hybrids are composed of the Fe_3O_4 and HBCuPc.

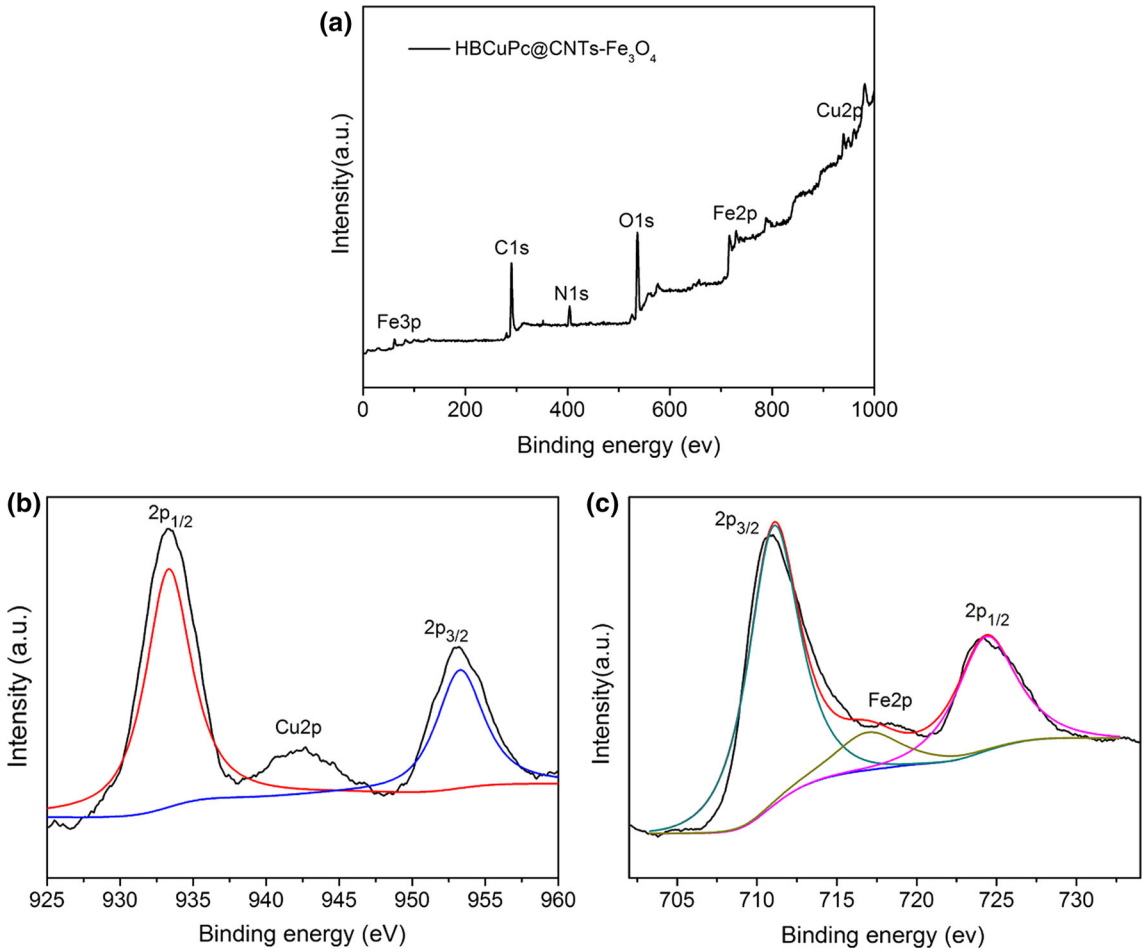

Fig. 3. (a) XPS scanned spectrum of HBCuPc@CNTs-Fe_3O_4; (b) Cu 2p peaks and (c) Fe 2p peaks of HBCuPc@CNTs-Fe_3O_4, respectively.

Dispersion of HBCuPc@CNTs-Fe_3O_4 in the PEN Matrix

According to the literature,[1,34] the mechanical, electrical, and thermal properties of composites are greatly influenced by the dispersibility of CNTs and the chemical affinity with the surrounding polymer matrix. Therefore, the fracture surfaces of the PEN/HBCuPc@CNTs-Fe_3O_4 composite films were investigated by SEM and are shown in Fig. 4. It also can be seen from the SEM images of pure PEN that the cross-sectional exhibited typical ductile dimple fracture features. With increasing HBCuPc@CNTs-Fe_3O_4 content, the morphology of the fracture surface gradually turned into brittle fracture. Most importantly, the phase interfaces between CNTs-Fe_3O_4 and PEN matrix are almost ambiguous, indicating good compatibility between CNTs-Fe_3O_4 particles and the PEN matrix. This may be attributed to the following reasons. Firstly, the dispersibility and compatibility of CNTs-Fe_3O_4 in the PEN matrix can be improved by the modifying of HBCuPc on the surface of CNTs-Fe_3O_4 (as shown in Fig. 4b and c), due to their similar structures and the strong intermolecular interactions between the terminal cyano of HBCuPc and the pendant nitrile groups on aromatic rings in PEN. Figure 4d shows the cross-section SEM images of the PEN/CNTs-Fe_3O_4 composite films containing 2 wt.% unmodified CNTs-Fe_3O_4. The result showed that the phase interface between unmodified CNTs-Fe_3O_4 and PEN matrix was is not well completed and self-aggregation is obvious. Besides, the modification of Fe_3O_4 on the surface of CNTs acts as a "rivet", enhancing the interlocking molecules chains and physical entanglement with the surrounding PEN matrix in a larger region, promoting a good interfacial adhesion between the CNTs-Fe_3O_4 and the PEN matrix.

Linear Viscoelastic Behaviors of the PEN/HBCuPc@CNTs-Fe_3O_4 Composite Films

Generally, the melt rheology of polymer-based composites not only predicts the dynamics, structure–property relationship and interaction between fillers and polymer matrix in the composite systems, but also provides theoretical guidance for the

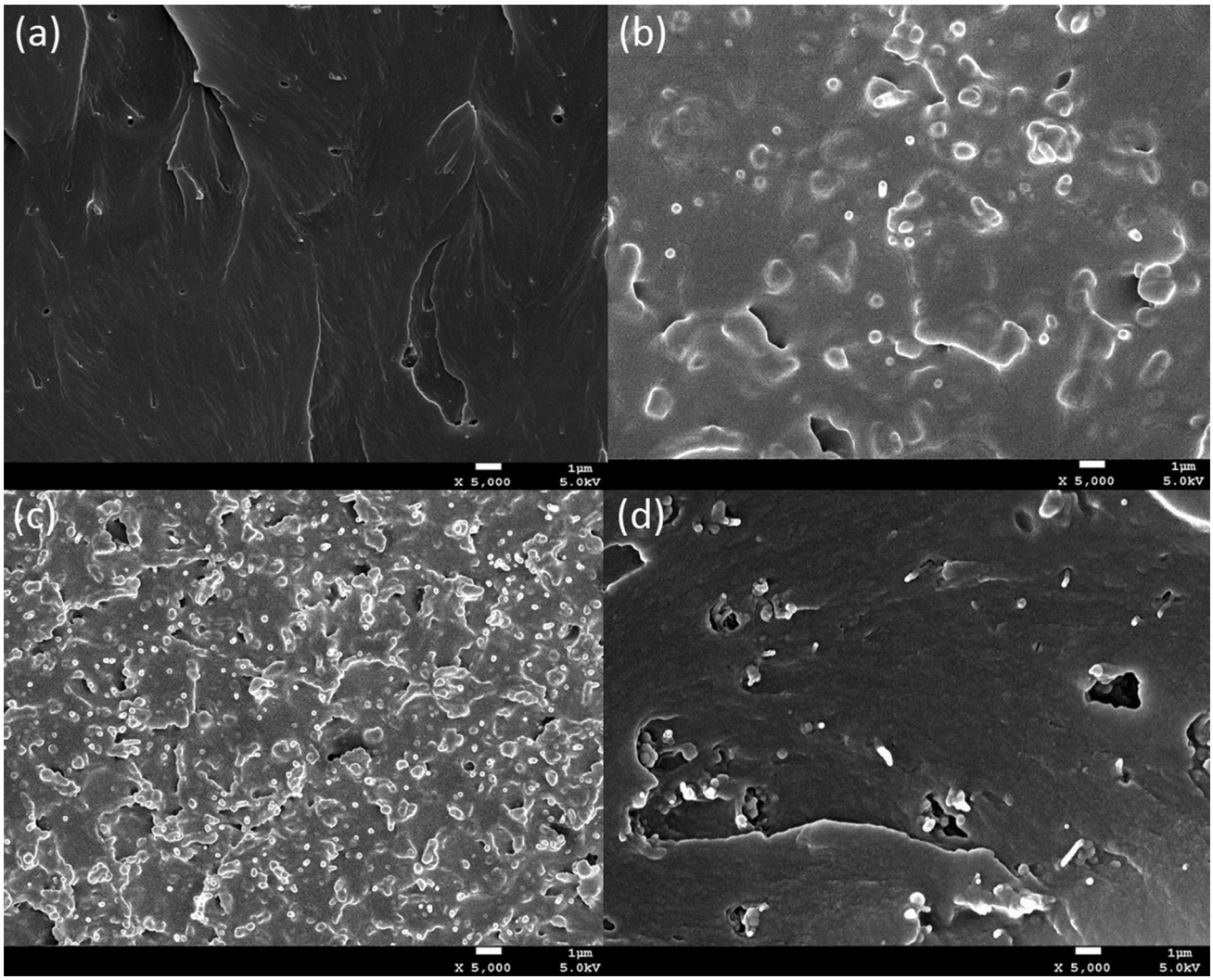

Fig. 4. Cross-sectional SEM images of PEN composite films with different HBCuPc@CNTs-Fe_3O_4 loading: (a) 0 wt.%, (b) 2 wt.% and (c) 10 wt.%; (d) with 2 wt.% unmodified CNTs-Fe3O4 loading.

polymer composites processing.[35,36] Firstly, the dynamic strain sweep is performed to determinate the linear viscoelastic region of the pure PEN and PEN composite films. The date for the isothermal oscillatory shear experiments of pure PEN conducted at 300°C, 320°C, and 340°C are shown in Fig. 5a. The linear region shifts to much higher strain values when temperature shifts from 300°C to 320°C, but the curves at 320°C and 340°C showed a similar trend. Therefore, the temperature of the subsequent dynamic rheological test was fixed at 320°C. The sweep curves of pure the PEN and the PEN composite with 3 wt.% HBCuPc@CNTs-Fe_3O_4 at 320°C are shown in Fig. 5b. It can be seen that the region of linear viscoelastic behavior has obviously changed in the presence of functionalized CNTs. However, the deviation from linear behavior for PEN/HBCuPc@CNTs-Fe_3O_4 composites occurs at a strain of more than 1%, which is in accordance with the previous work.[37] Thus, the latter rheological tests of all samples were conducted at a strain of 1%.

Figure 6a and b show the dependence of dynamic storage modulus (G') and loss modulus (G'') for PEN composite films with the different loading of HBCuPc@CNTs-Fe_3O_4, respectively. At low frequencies, it can be seen from Fig. 6b that pure PEN polymer chains are fully relaxed and present typical terminal behaviour with the scaling properties of about $G' \propto \omega^2$, which is consistent with the Cox-Merz rule.[38] With the increase of HBCuPc@CNTs-Fe_3O_4 content; however, the dependence of low frequency weakens and the increment of G' is more obvious, confirming the presence of strong interactions between CNTs and the PEN matrix. On the other hand, the change in the modulus is also attributed to the large scale PEN polymer relaxations that are restrained by the presence of HBCuPc@CNTs-Fe_3O_4 effectively,[39] which may be detailed as physical entanglement

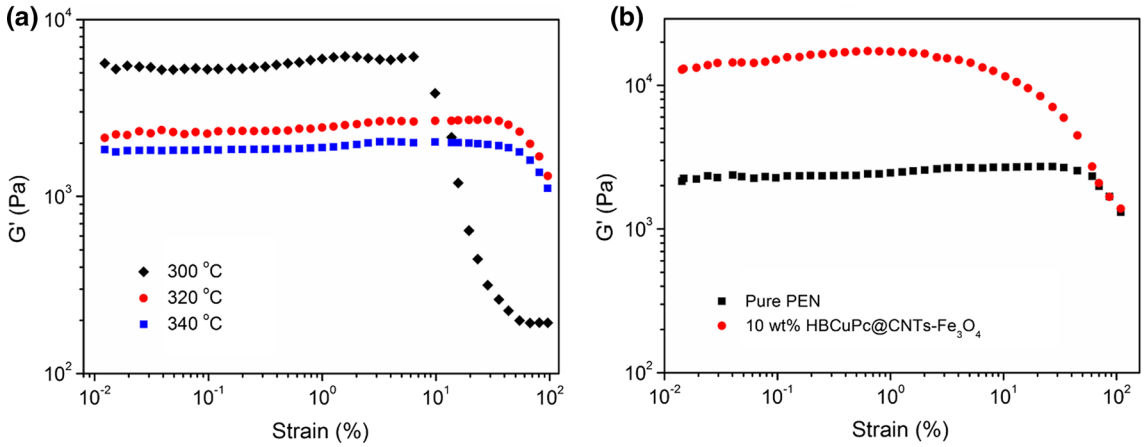

Fig. 5. (a) storage modulus (G') for pure PEN obtained in dynamic strain sweeps at 300°C, 320°C, and 340°C, (b) G' for pure PEN and 10 wt.% PEN/HBCuPc@CNTs-Fe_3O_4 composite films obtained in dynamic strain sweeps at 320°C.

and chemical interfacial interactions. In this case, the rough surface of CNTs could increase the knotting with the PEN chain.[40] In addition, the strong polar -CN on the functionalized CNTs-Fe_3O_4 also can interact with the PEN matrix. Thus, the same trend is observed in Fig. 6b for the *G"* curves.

Figure 6c shows the dependence of complex viscosity (η^*) for PEN composite films. It can be seen that the η^* of pure PEN shows little frequency dependence and almost behaves like a Newtonian fluid. Meanwhile, at low frequency, the PEN composite films below 6.0 wt.% HBCuPc@CNTs-Fe_3O_4 content show almost the same slope of η^* versus frequency. With further addition of HBCuPc@CNTs-Fe_3O_4, the Newtonian plateau of the viscosity curve disappears gradually, and the magnitude of η^* for PEN composite films abruptly increase, especially at low frequency, which is also attributed to the formation of the percolated structure by the fillers.[35,37] That is, a transition from viscoelastic liquid- to solid-like behavior has been formed in the PEN composites and the particle-particle interactions began to play a dominant role in the viscoelastic behavior. Figure 6d presents the relationship between *G'* at 0.10 rad/s for PEN composite films with the different loading of HBCuPc@CNTs-Fe_3O_4. Clearly, the magnitude of *G'* dramatically increases between 4 wt.% and 6 wt.% loadings, intuitively indicating that a filler network was formed in the composites with the increase of HBCuPc@CNTs-Fe_3O_4 content. As a result, a transient network, the so-called rheological percolation structure, can be formed when the content of fillers reaches high loading levels. Thus, the Newtonian plateau for η^* disappears, and the shear-thinning behavior becomes obvious, as can be seen in Fig. 6c.

Figure 7 shows the *G'* and *G"* for the PEN composite films with CNTs-Fe_3O_4 at identical loading levels of 2.1 wt.% and 5.5 wt.%, respectively. With the increase of functionalized CNTs content, the *G'* and *G"* incremental has changed significantly, especially in low frequency, which is attributed to the reinforcement effect of functionalized CNTs. Most importantly, the *G'* and *G"* of PEN/HBCuPc@CNTs-Fe_3O_4 composite films at identical filler loading is much higher than that of PEN/CNTs-Fe_3O_4 composite, which is strongly depended on the dispersion state of functionalized CNTs and interfacial interaction. At relative lower CNTs-Fe_3O_4 loadings of 2.1 wt.%, all composite films show higher *G"* than *G'* at low-frequency region, indicating that the relaxation behavior is still dominated by the local PEN dynamics. Thus, all samples showed obvious liquid viscoelastic behavior, as can be seen in Fig. 7a. At relative higher CNTs-Fe_3O_4 loadings of 5.5 wt.%, the PEN/HBCuPc@CNTs-Fe_3O_4 composite films show higher *G'* than *G"* at a lower frequency region, and a crossover point between *G"* and *G'* curves is observed from Fig. 7b, while this cannot be discovered from the PEN/CNTs-Fe_3O_4 samples, which reveals that PEN/HBCuPc@CNTs-Fe_3O_4 composite films have formed a rheological percolation structure and present solid-like behavior. This may be attributed to the following two reasons. On the one hand, both HBCuPc and PEN have abundant nitrile groups (-CN) with strong polarity, which show strong interfacial interaction between HBCuPc and PEN; thus, it can promote the affinity between HBCuPc@CNTs-Fe_3O_4 and the PEN matrix. On the other hand, the spherical Fe_3O_4 on the surface of CNTs could increase the interlock with the PEN matrix, thus effectively restrained the motion of PEN chains. As a result, the rheological response of interfacial elasticity of the PEN/HBCuPc@CNTs-Fe_3O_4 is more obvious than the PEN/CNTs-Fe_3O_4 system.

The Cole–Cole plots of the dynamic rheological test are used to describe the viscoelastic behavior (viscosity, modulus) of heterogeneous polymeric systems with the relaxation time distribution.[39] As shown in Fig. 8, the semicircular curve of the pure

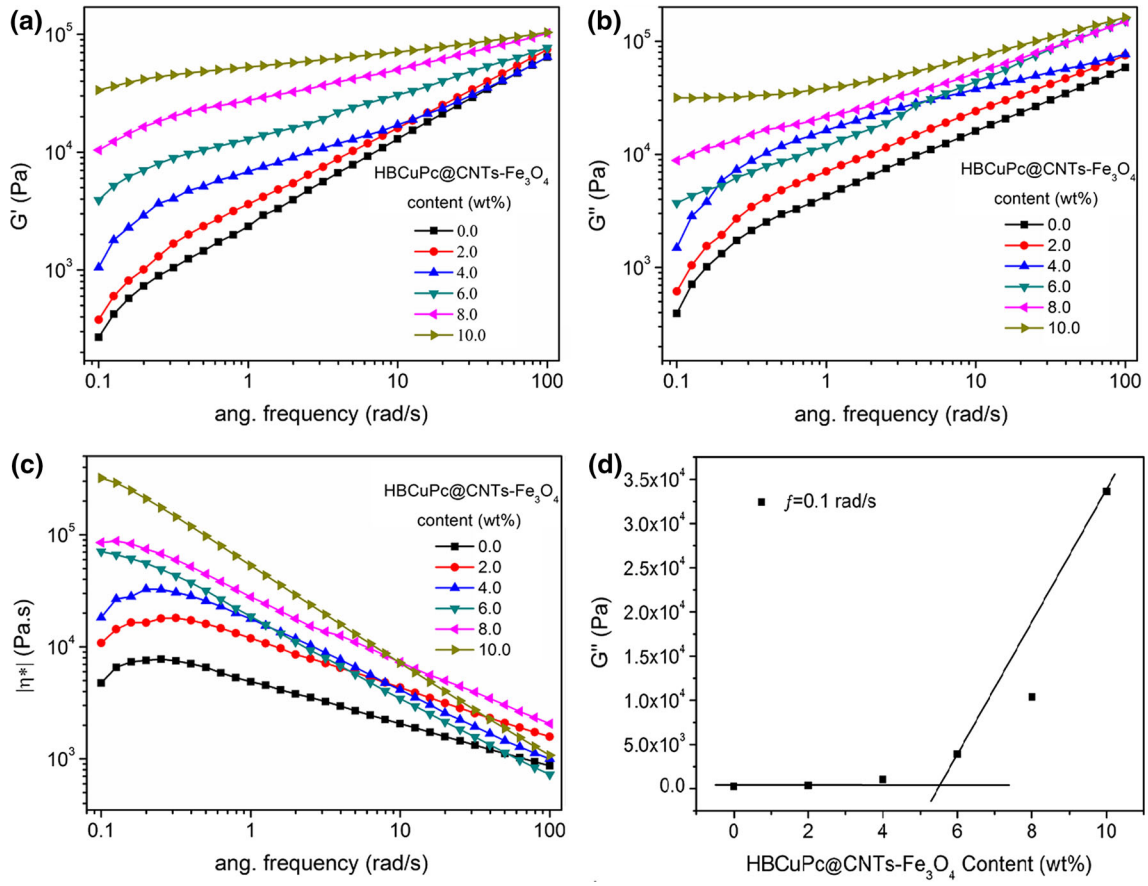

Fig. 6. (a) Dynamic storage modulus (G'), (b) loss modulus (G'') and (c) complex viscosity (η^*) for PEN composite films with the different loading of HBCuPc@CNTs-Fe3O4; (d) the plots of dynamic Storage modulus (G') at 0.10 rad/s versus HBCuPc@CNTs-Fe3O4 loadings.

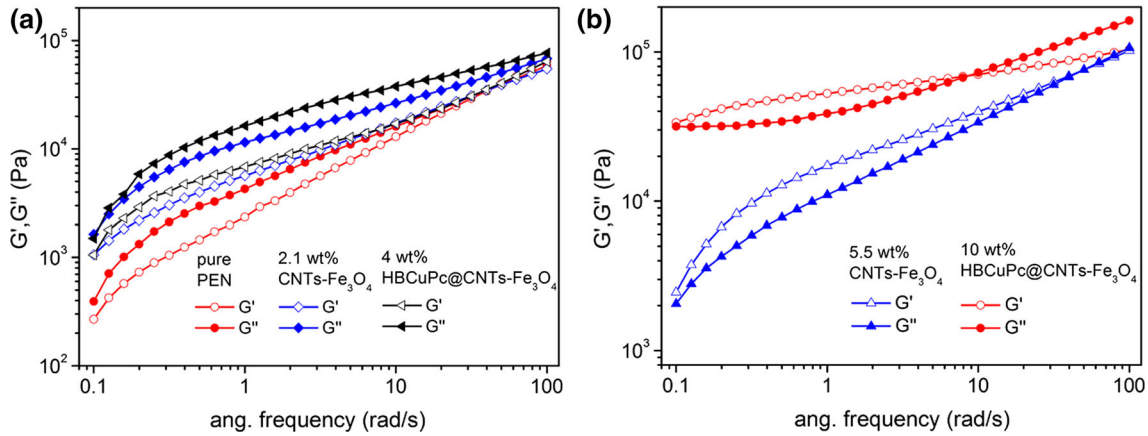

Fig. 7. The dynamic storage modulus (G') and loss modulus (G'') for the composite films with CNTs-Fe_3O_4 at identical loading levels of (a) 2.1 wt.% and (b) 5.5 wt.%.

PEN represents a relaxation process with a relaxation time distribution. With the addition of the HBCuPc@CNTs-Fe_3O_4, the semicircular curve becomes small gradually. As the loading level is more than 6 wt.%, the semicircular curve of PEN nearly disappears and approximates a straight line. The result indicated that the rheological percolation structure has been formed at present CNTs loadings, and the long-range motion of PEN chains is highly impeded as a result.

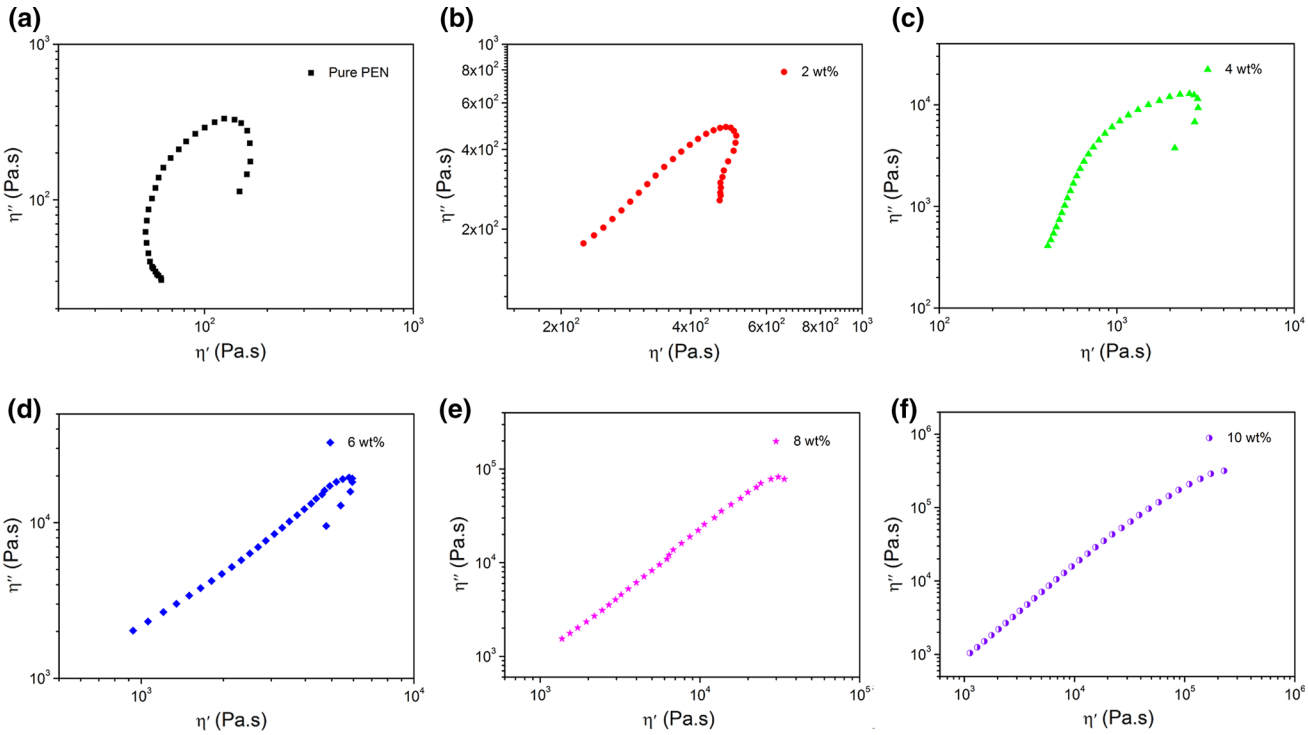

Fig. 8. Cole–Cole plots of imaginary viscosity (η'') versus real viscosity (η') for the pure PEN and PEN/HBCuPc@CNTs-Fe_3O_4 composite films: (a) 0 wt.%, (b) 2 wt.%, (c) 4 wt.% (d) 6 wt.%, (e) 8 wt.%, (f) 10 wt.%.

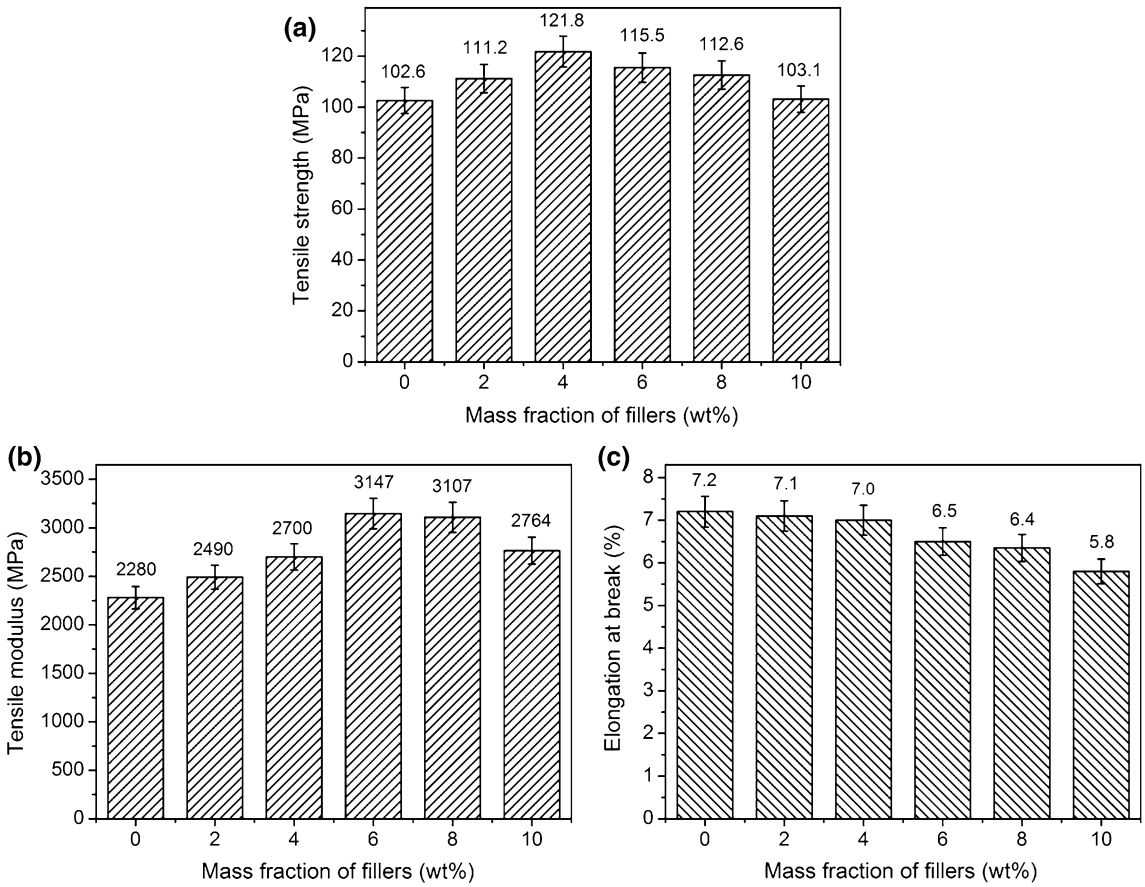

Fig. 9. Mechanical properties of the PEN/HBCuPc@CNTs-Fe_3O_4 composite films with different loading of filler: (a) tensile strength, (b) tensile modulus and (c) elongation at break.

Table I. Thermal properties of PEN/HBCuPc@CNTs-Fe_3O_4 composite films

Films	0 wt.%	2 wt.%	4 wt.%	6 wt.%	8 wt.%	10 wt.%
T_g (°C)	201	205	206	206	207	209
$T_{5\%}$ (°C)	481.0	484.2	484.6	479.3	483.1	488.4
T_{max}(°C)	511.7	512.5	513.2	513.4	514.2	516.7

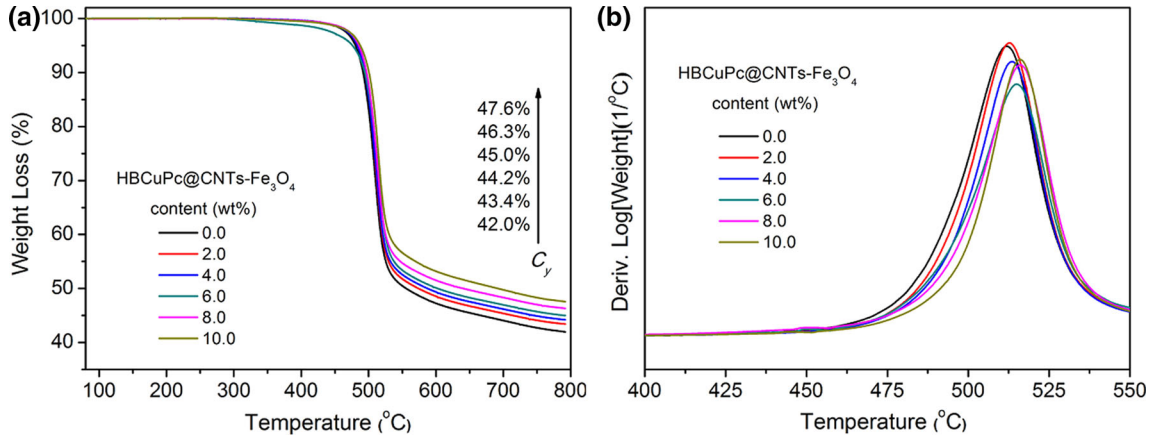

Fig. 10. (a) TGA and (b) DTG curves of pure PEN and PEN/HBCuPc@CNTs-Fe_3O_4 composite films.

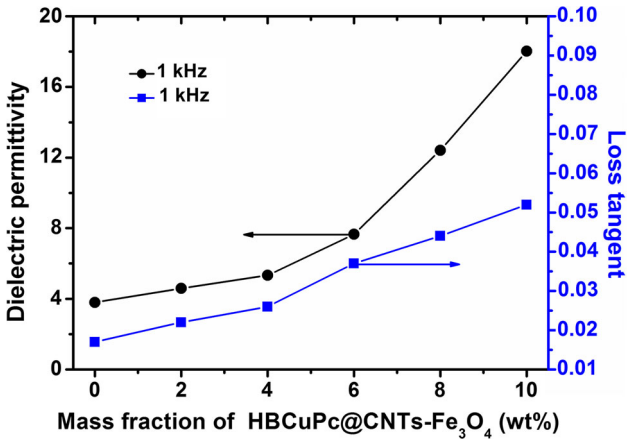

Fig. 11. Dielectric properties of PEN composite films with the different loading of HBCuPc@CNTs-Fe_3O_4 at 1 kHz.

Mechanical Properties of PEN/ HBCuPc@CNTs-Fe_3O_4 Composite Films

Figure 9 shows the effect of functionalized CNTs on the mechanical properties of PEN composite films. With the increasing of fillers content, the reinforcement efficiency of the functionalized CNTs was obviously changed. Significantly, for the 4 wt.% HBCuPc@CNTs-Fe_3O_4 reinforced PEN composite films, the tensile strength and modulus of PEN composite films increased 18.7% and 18.4% in comparison with those of pure PEN, respectively. The improvement is mainly attributed to the good dispersibility and compatibility of HBCuPc@CNTs-Fe_3O_4 particles in the PEN matrix, as observed in SEM (as can be seen from Fig. 4). However, the tensile strength decreases with higher HBCuPc@CNTs-Fe_3O_4 content (>4 wt.%) while tensile modulus reaches its highest value of 3147 MPa with 6 wt.% HBCuPc@CNTs-Fe_3O_4 and then decrease gradually, but they almost remain higher than that of pure PEN (as can be seen from Fig. 9a and b). As shown in Fig. 9c, the elongation at break of the PEN composite films decrease; but the elongation at break of 10 wt.% HBCuPc@CNTs-Fe_3O_4 content is still more than 5.8%. In a word, these results indicated that functionalized CNTs can present an outstanding enhancement effect on the mechanical properties of PEN in low content.

Thermal Properties of PEN/HBCuPc@CNTs-Fe_3O_4 Composite Films

DSC analysis was used to estimate the thermally induced phase transition behavior of pure PEN and PEN composite films. As summarized in Table I, all the composite films have a higher glass transition temperature (T_g) in comparison with pure PEN, and their T_gs gradually rise from 201°C to 209°C, with the increase of HBCuPc@CNTs-Fe_3O_4 content. In addition, the decomposition temperature at weight loss 5% ($T_{5\%}$) and the temperature corresponding to the maximum rate of decomposition (T_{max}) are also significantly higher than that of pure PEN (as can be seen from Fig. 10). For 10 wt.% HBCuPc@CNTs-Fe_3O_4 reinforced PEN composite films, the $T_{5\%}$ and

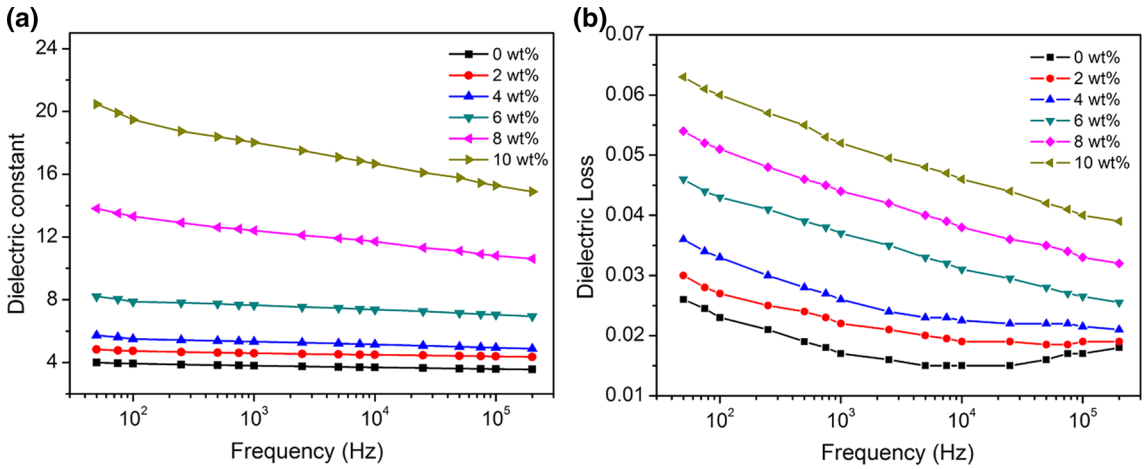

Fig. 12. Frequency dependences of (a) dielectric constant and (b) dielectric loss of the PEN composite films with the different loading of HBCuPc@CNTs-Fe_3O_4.

T_{max} increased by 7°C and 5°C, respectively. This improvement may be attributed to the following reasons. Firstly, the strong polymer-CNTs interaction can reduce free volume and segmental mobility, which can improve their T_gs. Secondly, good dispersion obviously improved the barrier effect of CNTs, thus the thermal conduction effect of CNTs became more effective for the increase of functional CNTs content.

Dielectric Properties of PEN/HBCuPc@CNTs-Fe_3O_4 Composite Films

Figure 11 shows the dielectric properties of PEN composite films with the different loading of HBCuPc@CNTs-Fe_3O_4 at 1 kHz. It is worth noticing that the dielectric properties of composite films are strongly enhanced by the introduction of functional CNTs. For instance, at 1 kHz, the permittivity (ε) of 10 wt.% HBCuPc@CNTs-Fe_3O_4 composite film presents a 4.7-fold increase (up to 18 from 3.8 of pure PEN). Most importantly, the size agglomeration of CNTs was improved in polymers after chemical modification, thereby effective blocking off the CNTs-CNTs contacts and providing a chance to rebuild the conductive network. Therefore, all the PEN composite films show a high permittivity and very low dielectric loss; their dielectric loss (tan δ) is still less than 0.051, even in the case of functionalized CNTs content up to 10 wt.%.

Furthermore, Fig. 12 shows the frequency-dependence of dielectric properties of the PEN composite films. When the content of HBCuPc@CNTs-Fe_3O_4 is low, it can be seen that the permittivity of the composite films is nearly independent of frequency (Fig. 12a). Besides, the dielectric loss of the composite films exhibits a slight decrease in the low frequency region, and then remains relatively constant at frequencies over 10 kHz (Fig. 12b). Nonetheless, with high HBCuPc@CNTs-Fe_3O_4 loading, the dielectric constant and loss decreased obviously with the increasing of frequency. Even for the composite containing 10 wt.% HBCuPc@CNTs-Fe_3O_4 loading, its dielectric constant and loss is still within a relatively low range, with the fluctuation range of 14.9–20.4 and 0.039–0.063, respectively. These results indicate that the functionalized CNTs serves to enhance the dielectric constant while retaining ultralow dielectric loss. This improvement may be attributed to the good compatibility and homogenous dispersion of functionalized CNTs in the PEN matrix. According to the micro-capacitor model,[41–43] the expected number of micro-capacitors in the polymer-based composites will be significantly increased because of the good homogeneity of the functionalized CNTs, leading to increased dielectric constants.

CONCLUSIONS

In conclusion, polymer-based flexile composite films were fabricated by using core–shell structured HBCuPc@CNTs-Fe_3O_4 hybrids as fillers and PEN as the polymer matrix, in which the conductive magnetic CNTs coaxials were coated by dielectric layers (HBCuPc). The results indicated that the HBCuPc-functionalized magnetic CNTs possess better dispersibility and interfacial adhesion in the PEN matrix. Besides, due to the effective blocking off of conductive paths by the organic semiconductor layers, the composite films show a high permittivity and very low dielectric loss, and the permittivity of the composite films is nearly independent of frequency. As a result, the PEN/HBCuPc@CNTs-Fe_3O_4 composite film shows a relatively high permittivity of 18 and a quite low dielectric loss of 0.051 (1 kHz) at aHBCuPc@CNTs-Fe_3O_4 concentration of 10 wt.%. The results of the melt rheology show that PEN/HBCuPc@CNTs-Fe_3O_4 presents a typical solid-like behavior, and the percolation threshold is about 5.5 wt.%. Furthermore, the composite films also showed outstanding thermal stability ($T_{5\%}$>480°C), high

tensile strength (more than 103 MPa) and good flexibility. In short, this study opens a good approach for functionalized CNTs and broadens the application fields of polymer-CNTs composites.

ACKNOWLEDGEMENT

The authors are thankful for the financial support from the National Natural Science Foundation of China (Project No. 51373028), the Sichuan University of Science and Engineering Talent Introduction Project (Nos. 2016RCL35, 2015RC56) and Material Corrosion and Protection Key Laboratory of Sichuan Province Open Fund Projects (2016CL16).

REFERENCES

1. Z. Dang, Y. Lin, H. Xu, C. Shi, S. Li, and J. Bai, *Adv. Funct. Mater.* 18, 1509 (2008).
2. K.I. Park, M. Lee, Y. Liu, S. Moon, G.T. Hwang, G. Zhu, J.E. Kim, S.O. Kim, D.K. Kim, Z. Wang, and K.J. Lee, *Adv. Mater.* 24, 2999 (2012).
3. Z. Dang, T. Zhou, S. Yao, J. Yuan, J. Zha, H. Song, J. Li, Q. Chen, W. Yang, and J. Bai, *Adv. Mater.* 21, 2077 (2009).
4. P. Khanchaitit, K. Han, M.R. Gadinski, Q. Li, and Q. Wang, *Nat. Commun.* 4, 1 (2013).
5. Y.B. Cohen, *J. Spacecraft Rockets* 39, 822 (2002).
6. X. Zhang, H. Chen, Y. Ma, C. Zhao, and W. Yang, *Appl. Surf. Sci.* 277, 121 (2013).
7. J.W. Xu and C. Wong, *Compos. A* 38, 13 (2007).
8. Q. Li, P. Peng, G.X. Chen, and S.W. Yoon, *J. Mater. Chem. C* 2, 8216 (2014).
9. K. Yang, X. Huang, L. Fang, J. He, and P. Jiang, *Nanoscale* 6, 14740 (2014).
10. Y. Feng, W. Li, Y. Hou, Y. Yu, W. Cao, T. Zhanga, and W. Fei, *J. Mater. Chem. C* 3, 1250 (2015).
11. Z. Liu, Y. Feng, and W. Li, *RSC Adv.* 5, 29017 (2015).
12. S. Jana, S. Garain, S. Sen, and D. Mandal, *Phys. Chem. Chem. Phys.* 17, 17429 (2015).
13. H. Tang, P. Wang, P. Zheng, and X. Liu, *Compos. Sci. Technol.* 123, 134 (2016).
14. O.A. Al-Hartomy, A.A. Al-Ghamdi, F. Al-Salamy, N. Dishovsky, R. Shtarkova, V. Iliev, and F. El-Tantawy, *J. Mater. Chem.* 2, 116 (2012).
15. J. Yuan, S. Yao, A. Sylvestre, and J. Bai, *J. Phys. Chem. C* 116, 2051 (2012).
16. Y. Hazama, N. Ainoya, J. Nakamura, and A. Natori, *Phys. Rev. B* 82, 045204 (2010).
17. J. Kim, T. Kim, J. Suk, H. Chou, J. Jang, J. Lee, I. Kholmanov, D. Akinwande, and R. Ruoff, *Small* 10, 3405 (2014).
18. Y. Zhan, J. Yang, Y. Zhou, X. Yang, F. Meng, and X. Liu, *Mater. Lett.* 78, 88 (2012).
19. Z. Dang, Y. Lin, and C. Nan, *Adv. Mater.* 15, 1625 (2003).
20. F. Jin, M. Feng, X. Huang, C. Long, K. Jia, and X. Liu, *Appl. Surf. Sci.* 357, 704 (2015).
21. L. Wang and Z. Dang, *Appl. Phys. Lett.* 87, 042903 (2005).
22. X. Yang, Y. Zhan, J. Yang, J. Zhong, R. Zhao, and X. Liu, *J. Polym. Res.* 19, 9806 (2012).
23. Y. Chen, B. Lin, X. Zhang, J. Wang, C. Lai, Y. Sun, Y. Liu, and H. Yang, *J. Mater. Chem. A* 2, 14118 (2014).
24. Z. Pu, L. Tong, M. Feng, K. Jia, and X. Liu, *RSC Adv.* 5, 72028 (2015).
25. L. Tong, K. Jia, and X. Liu, *Mater. Lett.* 128, 267 (2014).
26. Y. Zhan, R. Zhao, Y. Lei, F. Meng, J. Zhong, and X. Liu, *App. Surf. Sci.* 257, 4524 (2011).
27. Z. Pu, L. Chen, Y. Long, L. Tong, X. Huang, and X. Liu, *Colloids Surf. A* 415, 125 (2012).
28. Z. Pu, X. Zhou, X. Yang, K. Jia, and X. Liu, *J. Magn. Magn. Mater.* 385, 368 (2015).
29. J. Mack and M.J. Stillman, *Coordin. Chem. Rev.* 219, 993 (2001).
30. T. Kobayashi, F. Kurokawa, N. Uyeda, and E. Suito, *Spectrochim. Acta. A* 26, 1305 (1970).
31. S. Şaşmaz, E. Ağar, and A. Ağar, *Dyes Pigments* 42, 137 (1999).
32. S. Şaşmaz, E. Ağar, and A. Ağar, *Phys. Chem. Chem. Phys.* 15, 13038 (2013).
33. F. Meng and X. Liu, *RSC Adv.* 5, 7018 (2015).
34. S.J.V. Frankland and V.M. Harik, *Surf. Sci.* 525, 103 (2003).
35. P. Pötschke, T.D. Fornes, and D.R. Paul, *Polymer* 43, 3247 (2002).
36. X. Yang, Y. Zhan, R. Zhao, and X. Liu, *J. Appl. Polym. Sci.* 124, 1723 (2012).
37. X. Yang, Z. Wang, Y. Zhan, J. Yang, Y. Zou, R. Zhao, and X. Liu, *Polym. Int.* 62, 629 (2013).
38. W. Cox and E. Merz, *J. Polym. Sci.* 28, 619 (1958).
39. D. Wu, L. Wu, M. Zhang, and Y. Zhao, *Polym. Degrad. Stabil.* 93, 1577 (2008).
40. H. Guo, Y. Zhan, Z. Chen, F. Meng, J. Wei, and X. Liu, *J. Mater. Chem. A* 1, 2286 (2013).
41. X. Huang, Z. Pu, L. Tong, Z. Wang, and X. Liu, *J. Mater. Sci.: Mater. Electron.* 23, 2089 (2012).
42. Z. Dang, L. Wang, Y. Yin, Q. Zhang, and Q. Lei, *Adv. Mater.* 19, 852 (2007).
43. X. Huang, P. Jiang, and L. Xie, *Appl. Phys. Lett.* 95, 242901 (2009).